

University of Dundee

## Synthesis and Anti-Inflammatory Activity of 2-Amino-4,5,6,7-tetrahydrobenzo[b]thiophene-Derived NRF2 Activators

Mak, Kit-Kay; Shiming, Zhang; Epemolu, Ola; Dinkova-Kostova, Albena T; Wells, Geoffrey; Gazaryan, Irina G

*Published in:*  
ChemistryOpen

*DOI:*  
[10.1002/open.202200181](https://doi.org/10.1002/open.202200181)

*Publication date:*  
2022

*Licence:*  
CC BY-NC

*Document Version*  
Publisher's PDF, also known as Version of record

[Link to publication in Discovery Research Portal](#)

### *Citation for published version (APA):*

Mak, K-K., Shiming, Z., Epemolu, O., Dinkova-Kostova, A. T., Wells, G., Gazaryan, I. G., Sakirolla, R., Mohd, Z., & Pichika, M. R. (2022). Synthesis and Anti-Inflammatory Activity of 2-Amino-4,5,6,7-tetrahydrobenzo[b]thiophene-Derived NRF2 Activators. *ChemistryOpen*, 11(10), [e202200181]. <https://doi.org/10.1002/open.202200181>

### **General rights**

Copyright and moral rights for the publications made accessible in Discovery Research Portal are retained by the authors and/or other copyright owners and it is a condition of accessing publications that users recognise and abide by the legal requirements associated with these rights.

- Users may download and print one copy of any publication from Discovery Research Portal for the purpose of private study or research.
- You may not further distribute the material or use it for any profit-making activity or commercial gain.
- You may freely distribute the URL identifying the publication in the public portal.

### **Take down policy**

If you believe that this document breaches copyright please contact us providing details, and we will remove access to the work immediately and investigate your claim.

# Synthesis and Anti-Inflammatory Activity of 2-Amino-4,5,6,7-tetrahydrobenzo[b]thiophene-Derived NRF2 Activators

Kit-Kay Mak,<sup>[a, b, c]</sup> Zhang Shiming,<sup>[c]</sup> Ola Epemolu,<sup>[d]</sup> Albena T. Dinkova-Kostova,<sup>[e, f]</sup> Geoffrey Wells,<sup>[g]</sup> Irina G. Gazaryan,<sup>[h, i, j]</sup> Raghavendra Sakirolla,<sup>[k]</sup> Zulkefeli Mohd,<sup>[a, b]</sup> and Mallikarjuna Rao Pichika<sup>\*[a, b]</sup>

This is the first study investigating the nuclear factor (erythroid-derived 2)-like 2 (NRF2) activity of compounds containing a new scaffold, tetrahydrobenzo[b]thiophene. Eighteen compounds were synthesised and confirmed their NRF2 activation through NQO1 enzymatic activity and mRNA expression of NQO1 and HO-1 in Hepa-1c1c7 cells. The compounds disrupted the interaction between Kelch-like ECH-associated protein 1 (KEAP1) and NRF2 via interfering with the KEAP1's Kelch domain. The compounds exhibited anti-inflammatory activity in *Escherichia coli* Lipopolysaccharide (LPS<sub>Ec</sub>)-stimulated RAW

264.7 cells. The anti-inflammatory activity of the compounds was associated with their ability to activate NRF2. The compounds reversed the elevated levels of pro-inflammatory cytokines (IL-1 $\beta$ , IL-6, TNF- $\alpha$ , and IFN- $\gamma$ ) and inflammatory mediators (PGE2, COX-2, and NF- $\kappa$ B). The compounds were metabolically stable in human, rat, and mouse liver microsomes and showed optimum half-life ( $T_{1/2}$ ) and intrinsic clearance ( $Cl_{int}$ ). The binding mode of the compounds and physicochemical properties were predicted via in silico studies.


## Introduction


Inflammation involves complex molecular pathways and plays a pivotal role in the aetiology of all chronic diseases. Individuals threatened with infections, tissue damage, allergens, irritants, or non-infectious diseases will innately show pathophysiological responses via inflammatory reactions.<sup>[1]</sup> The immune system will respond to the threat via a chain of anti-inflammatory

mechanisms.<sup>[2]</sup> Discovering effective anti-inflammatory drugs is still an unmet need and challenges medicinal chemists. Inflammatory responses at the cellular level are executed via classical and non-classical pathways. The classical pathway activation includes the degradation of a protein inhibitor of NF- $\kappa$ B transcription factor, which upon activation eventually leads to the increased expression of NF- $\kappa$ B as a feedback regulation. The non-classical pathway is executed through NIK-kinase

- [a] K.-K. Mak, Prof. Dr. Z. Mohd, Prof. Dr. M. R. Pichika  
Pharmaceutical Chemistry Department,  
International Medical University, 126 Jalan Jalil Perkasa 19, Bukit Jalil,  
57000, Kuala Lumpur, Malaysia  
E-mail: mallikarjunarao@imu.edu.my
- [b] K.-K. Mak, Prof. Dr. Z. Mohd, Prof. Dr. M. R. Pichika  
Centre of Excellence for Bioactive Molecules and Drug Delivery  
Institute for Research, Development, and Innovation (IRDI)  
International Medical University  
126 Jalan Jalil Perkasa 19  
Bukit Jalil, 57000, Kuala Lumpur (Malaysia)
- [c] K.-K. Mak, Z. Shiming  
School of Postgraduate Studies  
International Medical University  
126 Jalan Jalil Perkasa 19  
Bukit Jalil, 57000, Kuala Lumpur (Malaysia)
- [d] Dr. O. Epemolu  
Principal research scientist- in vitro/in vivo DMPK  
Charles River Laboratories Edinburgh Ltd  
Tranent, East Lothian, Scotland (UK)
- [e] Prof. Dr. A. T. Dinkova-Kostova  
School of Medicine  
Jacqui Wood Cancer Centre  
University of Dundee  
Dundee, Scotland (UK)
- [f] Prof. Dr. A. T. Dinkova-Kostova  
Departments of Medicine and Pharmacology and Molecular Sciences  
Johns Hopkins University  
Baltimore, MA (USA)

- [g] Dr. G. Wells  
UCL School of Pharmacy  
University College London  
London WC1N 1AX (UK)
- [h] Dr. I. G. Gazaryan  
Faculty of Biology and Biotechnology  
National Research University Higher School of Economics  
Moscow (Russia)
- [i] Dr. I. G. Gazaryan  
Department of Chemical Enzymology  
M.V. Lomonosov Moscow State University  
Moscow (Russia)
- [j] Dr. I. G. Gazaryan  
Department of Chemistry and Physical Sciences  
Pace University  
Pleasantville, NY (USA)
- [k] Dr. R. Sakirolla  
Department of Chemistry,  
Central University of Karnataka  
Gulbarga, Karnataka (India)

 Supporting Information for this article can be found under: <https://doi.org/10.1002/open.202200181>.

 © 2022 The Authors. Published by Wiley-VCH GmbH. This is an open access article under the terms of the Creative Commons Attribution Non-Commercial License, which permits use, distribution and reproduction in any medium, provided the original work is properly cited and is not used for commercial purposes.

activation and has no feedback regulation. The NF- $\kappa$ B pathway coordinates adaptive immunity, inflammation, and apoptotic cell death. NF- $\kappa$ B is a redox-sensitive transcription factor activated by reactive oxygen species, in addition to typical inflammatory stimuli.

The advancement in understanding the inflammatory pathways links them to activation of the antioxidant pathway regulated by nuclear factor erythroid 2-related factor 2 (NRF2).<sup>[3–7]</sup> NRF2 negatively controls the NF- $\kappa$ B signalling pathway by multiple mechanisms still under investigation.<sup>[8]</sup> The protein stability of NRF2, the master regulator of genetic antioxidant responses,<sup>[9]</sup> is constitutively regulated via its interaction with a redox sensor protein – Kelch-like ECH-associated protein 1 (KEAP1), an adapter in Cul III ubiquitin ligase complexes.<sup>[10]</sup> Chemical modification of redox-active cysteine residues in KEAP1 or competitive displacement of NRF2 from KEAP1 results in NRF2 stabilisation,<sup>[11,12]</sup> followed by the translocation of NRF2 into the nucleus and enhanced expression of genes encoding cytoprotective proteins and suppression of genes encoding pro-inflammatory proteins.<sup>[13]</sup> The upregulation of pro-inflammatory cytokines such as interleukin (IL)-6 and IL-1 $\beta$  transcription induced by *Escherichia coli* lipopolysaccharide (LPS<sub>Ec</sub>) was reported to be prevented by NRF2 activation.<sup>[14–16]</sup> Thus, it has become an approach to discovering new NRF2 activators as anti-inflammatory agents.

Various endogenous or exogenous stressors inhibit KEAP1 and result in NRF2 accumulation. In cruciferous vegetables like broccoli, sulforaphane is a classical NRF2 activator that inhibits KEAP1 by covalently binding to cysteine 151.<sup>[17]</sup> However, the flexible linear long-chain in the sulforaphane molecule and the presence of the isothiocyanate group make it target cysteine thiols in numerous proteins,<sup>[18,19]</sup> resulting in undesirable side effects.<sup>[20]</sup> In this study, we have attempted to develop non-electrophilic NRF2 activators by 1) restricting the chain's flexibility in sulforaphane via cyclisation to a cyclohexane ring and 2) replacing the isothiocyanate group in sulforaphane with amino thiophene. The concept of the design of tetrahydrobenzo[*b*]thiophene derivatives (THBTs) is shown in Figure 1. The THBTs were synthesised using microwave and investigated their NRF2 activation and anti-inflammatory activity ability using in vitro models.

## Results and Discussion

### Synthesis of THBTs

All target compounds were synthesised using the route shown in Scheme 1, and the results are tabulated in Table 1. Using

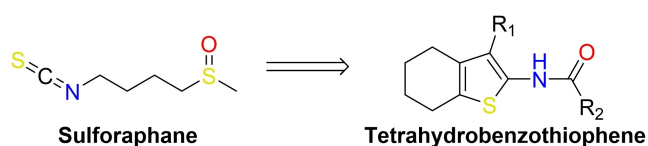
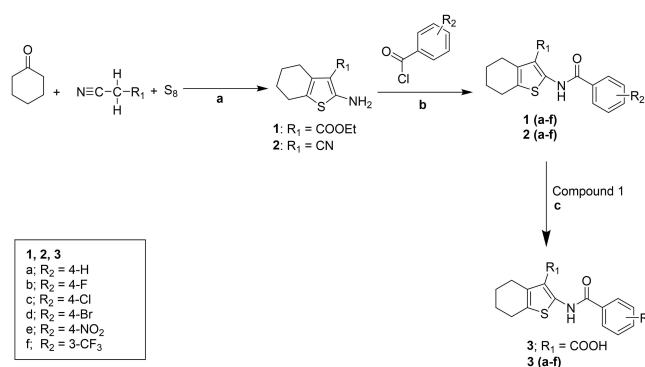


Figure 1. Design of tetrahydrobenzothiophene.



Scheme 1. General synthetic scheme for THBT derivatives. Reagents and conditions: (a) EtOH, diethylamine, 60 °C, 2 h; (b) pyridine, acid chloride, MV 400 Watts, 25 min, under nitrogen; (c) NaOH/EtOH, 85 °C, 1.5 h.

Table 1. The effect of THBTs on NO in LPS<sub>Ec</sub>-stimulated RAW264.7 cells.

Compound	R <sub>1</sub>	R <sub>2</sub>	NO Inhibition [%]
1a	-COOEt	-4-H	31.96 ± 8.17****
1b	-COOEt	-4-F	21.75 ± 9.35**
1c	-COOEt	-4-Cl	28.49 ± 8.45****
1d	-COOEt	-4-Br	24.22 ± 7.28***
1e	-COOEt	-4-NO <sub>2</sub>	11.97 ± 5.22 <sup>ns</sup>
1f	-COOEt	-3-CF <sub>3</sub>	10.11 ± 4.7**
2a	-CN	-4-H	78.04 ± 2.86****
2b	-CN	-4-F	41.94 ± 2.17****
2c	-CN	-4-Cl	33.35 ± 3.38****
2d	-CN	-4-Br	35.20 ± 9.38****
2e	-CN	-4-NO <sub>2</sub>	14.16 ± 4.75 <sup>ns</sup>
2f	-CN	-3-CF <sub>3</sub>	11.99 ± 0.24***
3a	-COOH	-4-H	87.07 ± 1.22****
3b	-COOH	-4-F	80.39 ± 5.89****
3c	-COOH	-4-Cl	64.74 ± 6.26****
3d	-COOH	-4-Br	44.26 ± 7.35****
3e	-COOH	-4-NO <sub>2</sub>	39.28 ± 6.51****
3f	-COOH	-3-CF <sub>3</sub>	44.58 ± 7.61****
<b>Sulforaphane [10 μM]</b>			<b>91.57 ± 11.76****</b>

Note: The NO production in RAW 264.7 cells by LPS<sub>Ec</sub> (negative control) is 100%. The data are expressed as the mean ± SD (n = 3). All the test compounds (except for 1e and 2e) have decreased the NO production to various degrees. The significance level of the results are indicated as such: \*p < 0.05, \*\*p < 0.01, \*\*\*p < 0.001, \*\*\*\*p < 0.0001 and <sup>ns</sup> = not significant.

Gewald's reaction, the key intermediates (1 and 2) were synthesised<sup>[21,22]</sup> via condensation of cyclohexanone, ethyl-2-cyanoacetate or malononitrile, and elemental sulfur. This reaction produces a 2-amino-THBT nucleus with an ethyl ester (1) or nitrile (2) at R<sub>1</sub>.<sup>[23]</sup>

The selective acylation of the thiophene amine was carried out using microwave irradiation.<sup>[24]</sup> In the literature, acylation of similar aminothiophenes using acid chlorides required long reaction times (4–12 h) at reflux and resulted in low yields (8–50%).<sup>[25,26]</sup> In this work, the microwave-assisted synthesis resulted in higher yields (71–88%) (1a–f (Series 1), 2a–f (Series 2)) and required a shorter duration of reaction (25 min).<sup>[27]</sup> Initially, compound 3 failed to form using cyano-

acetic acid in place of ethyl cyanoacetate in the first step. However, simple hydrolysis of the ethyl ester group at the C-3 position of series 1 with 1.0 M NaOH/EtOH solved the demise, producing compounds of **3 a–f** (Series 3).

### The cytotoxicity of THBTs

The cytotoxicity of the test compounds and standard compound (sulforaphane) to murine hepatoma (Hepa-1c1c7) and murine macrophage (RAW264.7) cells was determined using a well-established [3-(4,5-dimethylthiazol-2-yl)-2,5-diphenyltetrazolium bromide] (MTT) assay. The cytotoxicity of the *Escherichia coli* Lipopolysaccharide (LPS<sub>Ec</sub>) alone and together with either the test compounds or sulforaphane was tested on RAW 264.7 cells. The maximum concentration of sulforaphane used in this study is 10  $\mu\text{M}$ , whereas the maximum concentration of test compounds used is 100  $\mu\text{M}$ . The concentration of LPS<sub>Ec</sub> used in this study is 100  $\text{ng mL}^{-1}$ . Two-fold serial dilutions of the test compounds were made to produce different concentrations (100, 50, 25, 12.5, 6.25, 3.12, 1.56, and 0.78  $\mu\text{M}$ ). The sulforaphane (at 10  $\mu\text{M}$ ), LPS<sub>Ec</sub> (at 100  $\text{ng mL}^{-1}$ ), and test compounds (at 100  $\mu\text{M}$ ) did not show cytotoxicity on both cells. However, in the presence of LPS<sub>Ec</sub>, the test compounds were non-toxic to RAW264.7 cells until 50  $\mu\text{M}$ . The results are shown in the Supporting Information.

### The NRF2 activity of THBTs

The NRF2 activation effect of THBTs was determined by measuring the enzymatic activity of NAD(P)H quinone dehydrogenase 1 (NQO1), RNA expression of NQO1 and heme oxygenase 1 (HO-1), and inhibition of KEAP1-NRF2 interaction. The NQO1 enzymatic activity was carried out at different concentrations (100, 50, 25, 12.5, 6.25, 3.12, 1.56, and 0.78  $\mu\text{M}$ ) of test compounds, whereas the remaining activities were carried out at only one concentration (50  $\mu\text{M}$ ) of test compounds. The NQO1 enzyme activity was determined using Hepa1c1c7 following a well-established Prochaska bioassay method.<sup>[28]</sup> The expression of these two genes (NQO1 and HO-1) depends upon NRF2 activation.<sup>[29,30]</sup> The mRNA levels of the genes were quantified using the  $2^{-\Delta\Delta\text{Ct}}$  method<sup>[31]</sup> with  $\beta$ -actin as a reference gene. The ability of THBTs (at 50  $\mu\text{M}$ ) to disrupt NRF2 and KEAP1 interaction via the kelch domain of KEAP1 was assessed using a commercially available fluorescence polarisation assay kit.<sup>[32]</sup> The effect of THBTs on NQO1 activity is shown in Figure 2A, NQO1 expression in Figure 2B, HO-1 expression in Figure 2C, and KEAP1-NRF2 inhibition in Figure 2D.

The reference compound, sulforaphane, was the most potent, with a CD (concentration required to double the levels of NQO1) value of  $1.3 \pm 0.38 \mu\text{M}$ . Three THBTs (**3 a**, **3 b**, and **2 a**) are the most active compounds (Figure 2A), whose CD values are  $8.54 \pm 0.71 \mu\text{M}$ ,  $13.22 \pm 0.53 \mu\text{M}$  and  $64.32 \pm 1.04 \mu\text{M}$ , respectively, and their  $\text{IC}_{50}$  values are 14.78  $\mu\text{M}$ , 30.42  $\mu\text{M}$  and 46.52  $\mu\text{M}$  respectively. Compound **3 a** is the most potent,

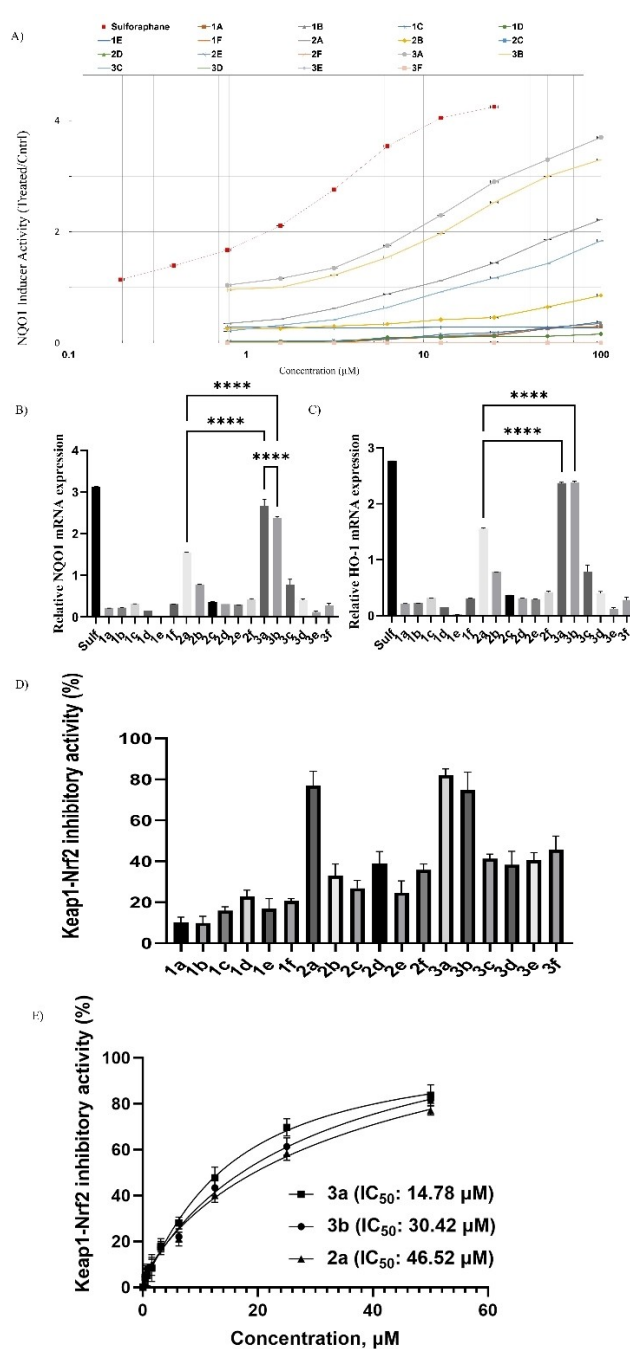


**Figure 2.** The effect of compounds on A) NQO1 activity, B) NQO1 gene expression, C) HO-1 gene expression, D) Keap1-NRF2 inhibitory activity, and E) dose-response (Keap1-NRF2 inhibition) curves of **2 a**, **3 a**, and **3 b**. The data are expressed as the mean  $\pm$  SD ( $n = 3$ ). The significance level of the results are indicated as such: \* $p < 0.05$ , \*\* $p < 0.01$ , \*\*\* $p < 0.001$ , \*\*\*\* $p < 0.0001$  and  $^{ns}$  = not significant.

whereas compound **2 a** is the least potent. A similar trend was observed in the expression of genes NQO1 (Figure 2B) and HO-1 (Figure 2C). **3 a** and **3 b** have upregulated the expression of both genes by 3-fold, whereas compound **2 a** has upregulated them by about 2-fold. The effect of compounds on the inhibition of KEAP1-NRF2 interaction (Figure 2D) followed the same trend observed in the NQO1 enzymatic assay and RNA

expression of NQO1 and HO-1. The compounds **3a**, **3b**, and **2a** are the most active, with inhibitions of  $82.07 \pm 3.06\%$ ,  $74.83 \pm 8.71\%$ , and  $64.98 \pm 7.01\%$ , respectively. All other compounds showed less than 50% inhibition.

### Anti-inflammatory activity of THBTs

NRF2/HO-1 is also involved in the modulation of inflammation, and it is believed that NRF2 activators could trigger the mechanism of action and escalate the anti-inflammatory process. The anti-inflammatory activity of the compounds was evaluated in LPS<sub>EC</sub>-induced inflammation in RAW 264.7 cells by measuring the nitric oxide (NO) production using the Griess assay.<sup>[32]</sup> The anti-inflammatory activity of the compounds was tested at 50  $\mu\text{M}$  concentration, and the results are shown in Table 1. The LPS<sub>EC</sub>-induced NO production was considered 100%, and the anti-inflammatory activity of THBTs was assessed by measuring their ability to reverse the LPS<sub>EC</sub>-induced NO production. All the tested compounds (except for **1e** and **2e**) have reversed the LPS<sub>EC</sub>-induced NO production. The THBTs **3a**, **3b**, and **2a** showed higher anti-inflammatory activity with an NO inhibition of  $87.07 \pm 1.22\%$ ,  $80.39 \pm 5.89\%$ , and  $78.04 \pm 2.86\%$ , respectively. All other THBTs inhibited NO production by less than 50%. Sulforaphane (10  $\mu\text{M}$ ), a reference compound, showed 91.57% NO inhibition. The anti-inflammatory activity of the THBTs followed a similar trend observed in their ability to activate NRF2.

### The effect of **3a**, **3b**, and **2a** on pro-inflammatory cytokines (IL-1 $\beta$ , IL-6, TNF- $\alpha$ , and IFN- $\gamma$ ) and inflammatory mediator (PGE2)

The above studies found that **3a**, **3b**, and **2a** possess the highest NRF2 activation and anti-inflammatory activities. So, the mechanism studies are investigated only for these three THBTs. The release of inflammatory mediators such as cytokines in inflammatory events is an innate response. The net effect of pro- and anti-inflammatory cytokines then modulates the inflammation.<sup>[33]</sup> However, the surge release of pro-inflammatory cytokines was associated with inflammatory diseases.<sup>[34,35]</sup> The effect of the THBTs (**3a**, **3b**, and **2a** at 50  $\mu\text{M}$ ) and sulforaphane (at 10  $\mu\text{M}$ ) on pro-inflammatory cytokines: interleukin (IL)-6, IL-1 $\beta$ , tumour necrosis factor-alpha (TNF- $\alpha$ ), and interferon-gamma (IFN- $\gamma$ ) and inflammatory mediator, prostaglandin E-2 (PGE2) was evaluated using commercially available ELISA microplates. The results are shown in Figure 3. LPS<sub>EC</sub> has upregulated all the cytokines and PGE2 in RAW264.7 cells, and its upregulation is assumed as 1. The THBTs reversed the LPS<sub>EC</sub>-induced levels of cytokines and PGE2. The compounds' activity is in the order of **3a** > **3b** > **2a**, and the trend is similar to that observed in NRF2 activation and anti-inflammatory studies.

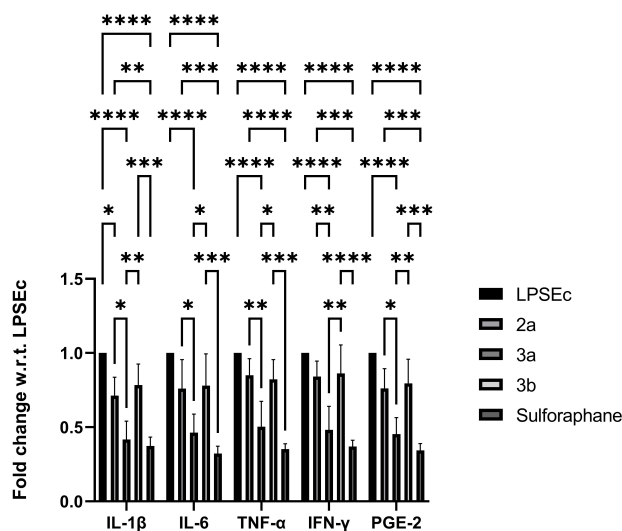


**Figure 3.** The effect of THBTs on pro-inflammatory cytokines and PGE2 in LPS<sub>EC</sub>-stimulated RAW 264.7 cells. The data are shown as the mean  $\pm$  SD ( $n = 3$ ). The effect of compounds on pro-inflammatory cytokines and PGE2 was determined by calculating the fold change with respect to (w.r.t.) negative control (LPS<sub>EC</sub>)-treated RAW 264.7 cells. The fold change by LPS<sub>EC</sub> is considered 1. All the NRF2-activating THBTs have downregulated the LPS<sub>EC</sub>-stimulated expression of pro-inflammatory cytokines and PGE2. The significance level of the results is indicated as such: \* $p < 0.05$ , \*\* $p < 0.01$ , \*\*\* $p < 0.001$ , \*\*\*\* $p < 0.0001$  and "no annotation" denotes the results are not significant.

### The effect of **3a**, **3b**, and **2a** on inflammatory mediators (NF- $\kappa$ B and COX-2)

The nuclear factor-kappa B (NF- $\kappa$ B) is an upstream regulator of inflammation, and its upregulation also upregulates the cyclooxygenase-2 (COX-2) expression. Detailed studies over the decades have shown that the modulation of upstream inflammatory regulators coupled with the neutralisation of inflammatory mediators and genes can effectively reduce inflammation.<sup>[36]</sup> The effect of compounds on COX-2 and NF- $\kappa$ B is shown in Figure 4.

### Metabolic stability of **3a**, **3b**, and **2a** in liver microsomes

The metabolic stability of the compounds was carried out in liver microsomes (mouse, rat, and human) to predict the in vivo dose and the right animal model.<sup>[37]</sup> The half-life ( $T_{1/2}$ ) and intrinsic clearance ( $Cl_{int}$ ) of the compounds were determined using the well-established protocol.<sup>[38]</sup> The results are shown in Table 2. The compounds have moderate to high intrinsic clearance ranging from 3.46 to 11.35 mL min<sup>-1</sup>/g liver, with  $T_{1/2}$  values ranging from 5.29 to 16.03 min. In human liver microsomes, the  $T_{1/2}$  values of **2a**, **3a**, and **3b** are 7.73, 12.59, and 11.14 min, respectively. In comparison, the  $T_{1/2}$  values in the rodents (mouse and rat) are in increasing order of **2a**, **3a**, and **3b**. The compounds were rapidly cleared in mice compared to rats and humans. Thus, the rat model (compared to the mouse model) could be the most appropriate model to test the in vivo activity of these compounds.

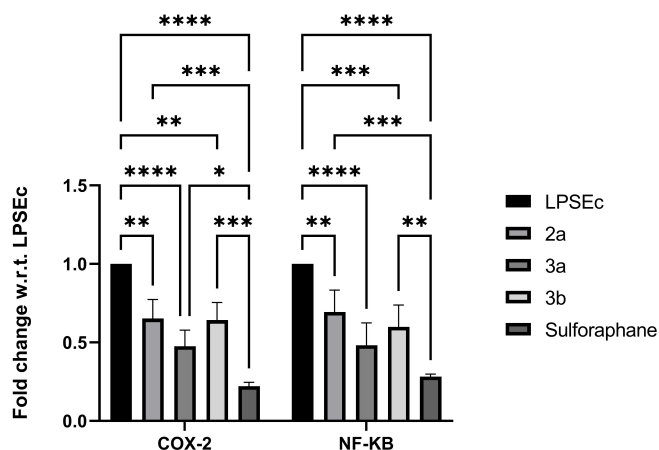


**Figure 4.** The effect of THBTs on COX-2 and NF- $\kappa$ B expression in LPS<sub>Ec</sub>-stimulated RAW 264.7 cells. The data are shown as mean  $\pm$  SD (n = 3). The effect of compounds on inflammatory regulators was determined by calculating the fold change with respect to (w.r.t.) negative control (LPS<sub>Ec</sub>-treated RAW 264.7 cells). All the compounds have downregulated the LPS<sub>Ec</sub>-stimulated expression of COX-2 and NF- $\kappa$ B. The significance level of the results is indicated as such: \*p < 0.05, \*\*p < 0.01, \*\*\*p < 0.001, \*\*\*\*p < 0.0001 and “no annotation” denotes the results are not significant.

### In silico studies

The in silico studies were carried out using Schrödinger Drug Discovery Suite 2021-4 software. The molecular interactions between the active compounds (**2a**, **3a**, and **3b**) and the amino acid residues in the KEAP1 Kelch domain were investigated via molecular docking studies, induced-fit docking studies, MM-GBSA calculations, and molecular dynamics<sup>[39]</sup> (MD, for 100 ns). The compounds were docked into the Kelch domain (PDB ID:

4IQK) of KEAP1. The docked poses were visually inspected, and the poses with the appropriate conformation were selected for induced-fit docking studies, MM-GBSA calculations, and MD simulations. The physicochemical and drug-like properties of the test compounds were also predicted.

The docking scores, binding energies, and drug-like properties of the compounds are shown in Table 3. The negative docking scores in molecular docking (g score) and induced-fit docking (g score and IFD score) studies suggested that the binding of these compounds in the Kelch domain of KEAP1 is favourable. The negative free binding energies (from MM-GBSA calculations) further confirm the stability of the compounds in the Kelch domain of KEAP1. The MD simulation results suggest that these compounds form a relatively stable complex with the Kelch domain of KEAP1. The compounds' physicochemical and drug-like properties are within the recommended range for oral drugs.<sup>[40]</sup> The key amino acid residues involved in the molecular interactions with the compounds (from molecular docking studies) are listed in Table 4. Figure 5 depicts the 2D- and 3D-poses of the compounds in the binding pocket of the Kelch domain of KEAP1 from molecular docking studies. Figure 6 depicts the results from MD simulations that include relative mean square deviation (RMSD) of the complex (Kelch domain with **2a**, **3a**, and **3b**), the amino acids that are involved in the interaction with the compounds, and the key atoms of the compounds involved in the binding. The full reports of the MD simulations were provided in the Supporting Information.

**Table 2.** The metabolic stability of THBTs in human, rat, and mouse liver microsomes.

Cpd <sup>[a]</sup>	Cl <sub>int</sub> [mL min <sup>-1</sup> /g liver] <sup>[b]</sup> HLM <sup>[d]</sup>	RLM <sup>[e]</sup>	MLM <sup>[f]</sup>	T <sub>1/2</sub> [min] <sup>[c]</sup> HLM <sup>[d]</sup>	RLM <sup>[e]</sup>	MLM <sup>[f]</sup>
Ver <sup>[g]</sup>	11.82 $\pm$ 0.07	14.72 $\pm$ 0.03	13.31 $\pm$ 0.08	6.34	5.29	5.74
<b>2a</b>	9.41 $\pm$ 0.03	5.52 $\pm$ 0.04	11.35 $\pm$ 0.03	7.73	13.18	6.41
<b>3a</b>	5.78 $\pm$ 0.02	5.47 $\pm$ 0.02	6.34 $\pm$ 0.03	12.59	13.30	11.48
<b>3b</b>	6.53 $\pm$ 0.02	4.54 $\pm$ 0.04	5.50 $\pm$ 0.03	11.14	16.03	13.23

[a] Cpd: compounds; [b] Cl<sub>int</sub>: intrinsic clearance; [c] T<sub>1/2</sub>: half-life; [d] HLM: human liver microsomes; [e] RLM: rat liver microsomes; [f] MLM: mouse liver microsomes; [g] Ver: Verapamil. The data are shown as mean  $\pm$  SD (n = 3).

**Table 3.** The docking scores, binding energies, and physicochemical and drug-like properties of THBTs.

XP docking gscore	Induced-fit docking			MM-GBSA $\Delta$ G	Physicochemical and Drug-like properties							
	gscore	IFD <sup>[a]</sup> Score	IFD <sup>[a]</sup> Score		QPlogPo/w <sup>[b]</sup>	QPlogS <sup>[c]</sup>	QPlogBB <sup>[d]</sup>	CNS <sup>[e]</sup>	QPCCaco <sup>[f]</sup>	QPlogHERG <sup>[g]</sup>	PercentHOA <sup>[h]</sup>	QPlogKhsa <sup>[i]</sup>
<b>3a</b>	-4.37	-6.94	-12886.35	-47.2	3.71	-4.43	-0.59	-1	194.53	-2.97	89.64	0.19
<b>3b</b>	-3.52	-7.66	-12892.36	-56.46	3.95	-4.80	-0.49	-1	194.89	-2.86	91.04	0.23
<b>2a</b>	-4.44	-6.08	-12844.38	-50.72	3.11	-5.55	-0.55	0	973.65	-5.23	100.00	0.26

[a] IFD: Induced Fit Docking; [b] QPlogPo/w: predicted octanol/water partition coefficient: recommended range -2.0 to 6.5; [c] QPlogS: prediction of aqueous solubility level: recommended range -6.5 to 0.5; [d] QPlogBB: predicted brain/blood partition coefficient: recommended range -3.0 to 1.2; [e] CNS: central nervous system activity: -2 = completely inactive, -1 = very low activity, 0 = low activity, 1 = medium activity, 2 = completely active; [f] QPCCaco: predicted apparent gut-blood barrier permeability: < 25 = poor, > 500 = good; [g] QPlogHERG: predicted IC<sub>50</sub> value for blockage of HERG K<sup>+</sup> channels: < -5 = concern; [h] PercentHOA: percentage of human oral absorption level: > 80% = high absorption, < 25% = poor absorption; [i] QPlogKhsa: prediction of binding to human serum albumin: -1.5 to 1.5.

Compound	H-bond interactions	Hydrophobic interactions	Van der Waal's interactions
2a	SER555	TYR525, ALA 556, TYR572	GLY364, ARG415, GLY462, ARG483, GLN530, GLY574, GLY603, GLY509,
3a	SER602	ILE416, ALA510, VAL463, VAL512, ALA556, LEU557	SER363, GLY364, ARG415, GLY416, GLY417, GLY464, GLY509, SER508, GLY511, ALA556, LEU557, SER602, GLY603
3b		VAL463, VAL465, ALA510, VAL512, ALA556, LEU557, ILE559, VAL604	ASN414, ARG415, GLY462, GLY464, SER363, GLY364, GLY558, GLY603, SER602,

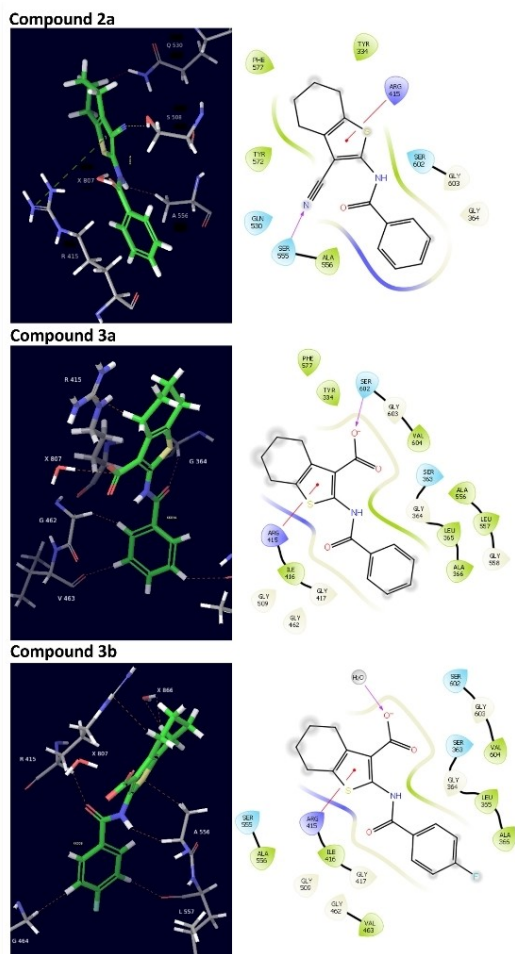


**Figure 5.** The molecular interactions (XP Glide docking) of **2a**, **3a**, and **3b** in the Kelch domain of KEAP1 (PDB ID: 4IQK). The first column shows the 3-dimensional (3D) interaction diagrams. The second column shows the 2D interactions (pink, hydrogen bond; red, cation bond) between the functional groups of the compounds with the specific amino acids.

## Conclusion

Eighteen compounds containing a new scaffold, tetrahydrobenzothiofene (THBT), were designed based on sulforaphane. Sulforaphane is the most potent natural NRF2 activator. It is an electrophilic activator. The isothiocyanate functional group in sulforaphane forms covalent interaction with the thiol group in CYS151 of KEAP1 and thus activates NRF2. At the same time, it

also reacts with cysteine thiols in numerous proteins. The carbon chain in sulforaphane is straight, and thus it is highly flexible. THBTs were designed so that the straight carbon chain and isothiocyanate group in sulforaphane were constrained in the form of fused bicyclic tetrahydrobenzothiofene.

The amino thiophene nucleus (**1** and **2**) was synthesised using Gewald's reaction. The series **1** (**1a–f**) and Series **2** (**2a–f**) compounds were synthesised via N-alkylation of **1** and **2** with acyl using microwave irradiation. Series **3** (**3a–f**) were synthesised by the hydrolysis of series **1** (**1a–f**). Compared to conventional reflux, microwave irradiation resulted in faster acylation and higher product yields with a purity of > 95%.

The NRF2 activation ability of the THBTs was preliminarily evaluated using Hepa-1c1c7 cells by determining their ability to induce NQO1 activity and upregulate the mRNA expression of NQO1. All the eighteen compounds were non-toxic to the Hepa-1c1c7 cells up to a concentration of 100  $\mu\text{M}$ . Three THBTs (**2a**, **3a**, and **3b**) had shown significant increase in NRF2 activation in the order of **3a** > **3b** > **2a**. The THBTs containing the ester group (ethyl carboxylate) on core moiety at C-2 did not activate NRF2, whereas the cyano and carboxyl group showed NRF2 activation. The substituents (fluoro, chloro, bromo, nitro, and trifluoromethyl) on the aromatic ring of the amide group have decreased the NRF2 activation. However, these compounds were not as potent as sulforaphane. Thus, the anti-inflammatory activity of these three THBTs (**2a**, **3a**, and **3b**) was further studied.

The anti-inflammatory activity of the compounds was evaluated using LPS<sub>EC</sub> challenged RAW 264.7 cells by measuring NO production, pro-inflammatory cytokines (IL-1 $\beta$ , IL-6, TNF- $\alpha$ , and IFN- $\gamma$ ), and inflammatory mediators (PGE<sub>2</sub>, COX-2, and NF- $\kappa$ B). All three THBTs had shown significant inhibition of NO, pro-inflammatory cytokines, and inflammatory mediators. The order of anti-inflammatory activity is the same as that shown in NRF2 activation. The compounds were non-toxic up to the concentration of 100  $\mu\text{M}$ . Since these compounds have shown promising anti-inflammatory activity, these compounds have further proceeded to metabolic stability studies.

The metabolic stability of these compounds was assessed using human, rat, and mouse liver microsomes and determined the intrinsic clearance and half-life. The compounds **3a** and **3b** were moderately stable in human and mouse microsomes. Therefore, mice can be used to confirm these compounds' in vivo NRF2 activation ability.

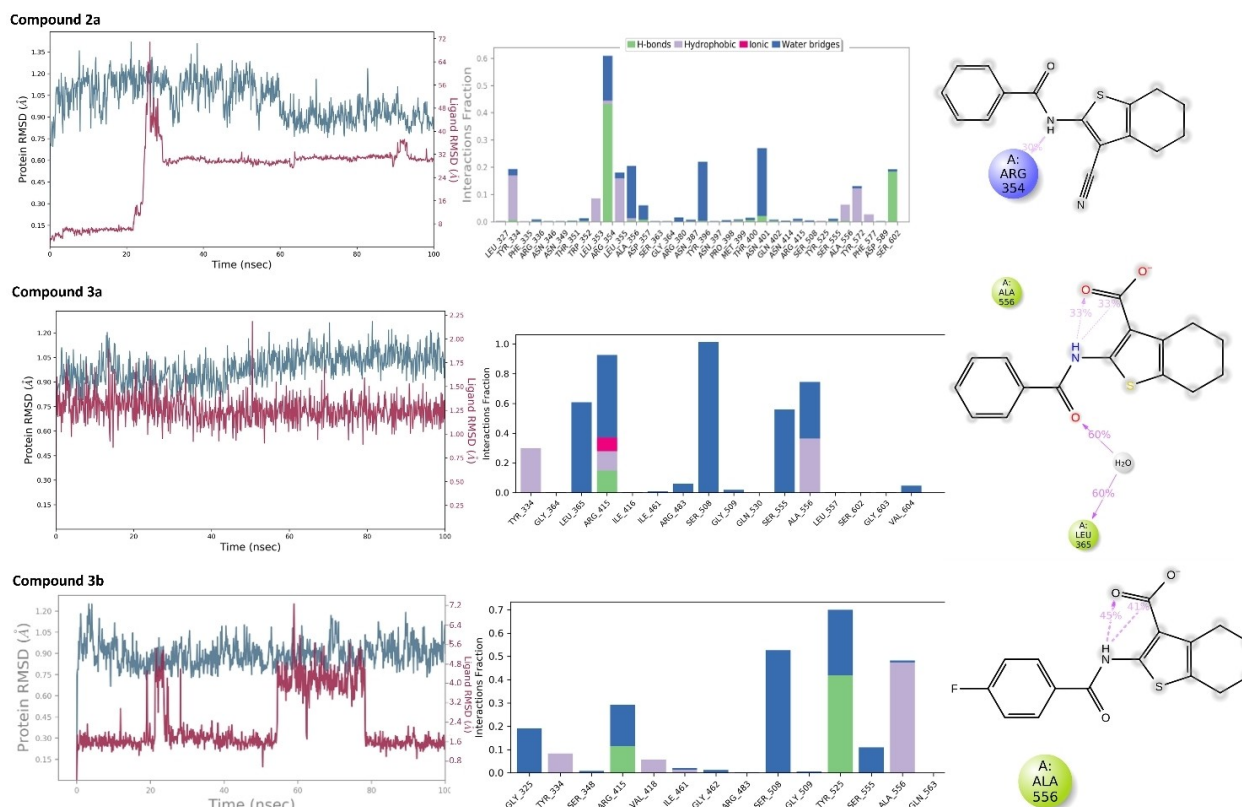


**Figure 6.** Molecular dynamics (MD) simulation (100 ns) of **2a**, **3a**, and **3b** complexes with the Kelch domain of KEAP1 (PDB ID: 4IQK). The first column depicts the protein-ligand complex's RMSD (root mean squared deviation) plots. The left y axis shows the RMSD values of the protein. The right y axis indicates the RMSD values of the compound with respect to the protein in its binding pocket. The RMSD changes of 1–3 Å units are considered acceptable. The protein-ligand complex for **3a** is stable throughout the MD simulation, whereas the protein-ligand complexes for **2a** and **3b** are not stable. The second column depicts the plot of protein interactions with the compounds. Compound **2a** mainly interacts with Arginine 354 (hydrogen bonding, water bridges, and hydrophobic interactions for 60% of the simulation time). The compound **3a** mainly interacts with Serine 508 (water bridges for 100% of the simulation time), Arginine 415 (water bridges, hydrogen bonding, hydrophobic and ionic bonding 90% of the simulation time), Alanine 556 (hydrophobic and water bridges for 55% of the simulation time), Leucine 385 (water bridges for 60% of the simulation time) and Serine 555 (water bridges for more than 55% of the simulation time). The third column shows the schematic of detailed atom interaction(s) with protein residue(s) for more than 30% of the simulation time. In **2a**, the amino group forms an interaction with Arginine 354 for 30% of the simulation time. In **3a**, the carbonyl of the amide group forms a water-mediated interaction with Leucine 365 for 60% of the simulation time. In addition, it also forms a hydrophobic interaction with Alanine 556 for > 30% of the simulation time. In **3b**, the aromatic ring forms a hydrophobic interaction with Alanine 556 for > 30% of the simulation time. The MD simulation studies showed that **3a** engages with the protein amino acids longer than that of **3b**, which is longer than **2a**. The order of interaction duration between the compounds and protein is **3a** > **3b** > **2a**, the same as that of NRF2 inducing activity.

The binding poses of the compounds in the KEAP1's kelch domain (PDB code: 4IQK) were determined using molecular docking and induced-fit docking studies, and the complexes' stability was determined using MD simulation studies. The docking scores for all three compounds were negative, suggesting the compounds form favourable interactions with the amino acids in the kelch domain. The favourable binding of the compounds with the kelch domain was further confirmed by the negative binding energies observed in MM-GBSA calculations. However, molecular dynamics studies have revealed that compound **3a** is more stable in the binding pocket compared to compounds **2a** and **3b**. **3a** is stable for the entire 100 ns simulation time. Compound **3b** is stable for about half of the simulation time (100 ns), whereas compound **2a** is not stable in the binding pocket. The MD simulations have provided insights into why compound **3a** is the most active NRF2 activator and anti-inflammatory compound.

## Experimental Section

### Chemicals and instruments for the synthesis of the compounds

All the chemicals and reagents for synthesis were purchased from Acros Organics. The compounds' melting point was recorded using Stuart Melting Point Apparatus, SMP11 (Cole Parmer, UK). The NMR spectra of the compounds were recorded on a Bruker 600 MHz spectrometer. The elemental analysis was performed using a CHN Elemental Analyzer (Perkin Elmer, USA).

### Synthesis of compounds

#### Ethyl-2-amino-4,5,6,7-tetrahydrobenzo[b]thiophene-3-carboxylate/carbonitrile/carboxylic acid (**1**, **2**)

Cyclohexanone (1 mmol) and ethyl cyanoacetate or malononitrile (1.2 mmol) were added to a clean beaker. The mixture was heated to 60 °C with stirring. To the mixture was added sulfur (1 mmol).



The mixture was allowed to stir for 2 h or until light orange crystals were observed. The progress of the reaction was monitored using thin-layer chromatography. The residue was filtered using Büchner filtration, washed with ethanol, and recrystallised from 95% ethanol. The yield of **1** is 78%, and that for **2** is 85%.

### Alkylation of the 4,5,6,7-tetrahydrobenzo[b]thiophene derivatives (**1**, **2**) at the amino group with acid chlorides via microwave synthesis

Zarecki et al. (41) adapted the green synthesis using microwave-synthesiser. To the microwave synthesiser vessel containing either **1** or **2** (1 mmol) in pyridine were added acyl chlorides (1.5 mmol). The mixture was clamped tight and placed in the microwave synthesiser with parameters of 400 W and 25 min holding time and stirring. Once the mixture cooled, the solids were vacuumed and recrystallised with 95% ethanol. The microwave synthesiser, Monowave™ 450 (Anton Paar GmbH, Germany), was used to synthesise six compounds in each series **1 a–f** and **2 a–f**. In general, the yield is >70%.

### Hydrolysis of ethyl ester group in the series of compounds **1** to form **3**

In a clean round bottom flask containing **1 a**, **1 b**, **1 c**, **1 d**, **1 e**, or **1 f**, was added 1.0 M NaOH in 95% ethanol. The ethyl ester group was then hydrolysed to carboxylic acid giving rise to the third series of compounds (**3 a–f**). The compound was filtered under vacuum using a Büchner filter, washed, and recrystallised with 95% ethanol. In general, the yield is >75%.

### Cell Culture

Murine macrophage, RAW264.7 cell line was purchased from American Type Culture Collection (ATCC, Manassas, USA). RAW 264.7 cells were cultured and maintained in Dulbecco's Modified Eagle's Medium (DMEM; Gibco, USA) supplemented with 10% fetal bovine serum (FBS; Sigma Aldrich, USA) and 1% penicillin-streptomycin (100 U mL<sup>-1</sup> penicillin and 100 µg mL<sup>-1</sup> streptomycin; Sigma Aldrich, USA). The cells were maintained in a 37°C and 5% CO<sub>2</sub> incubator.

### Preparation of the test compounds and Escherichia coli Lipopolysaccharide (LPS<sub>Ec</sub>)

The required amounts of test compounds and LPSEc were dissolved in molecular biology grade DMSO to prepare a 10 mM stock solution. The stock solution was diluted with phosphate buffer saline (PBS, pH 7.4) to produce the required concentrations of test solutions. In all in vitro experiments, the final concentration of DMSO was not more than 0.1% (v/v); thus, 0.1% DMSO in PBS was used as a vehicle.

### Effect of test compounds on cell viability

Vybrant® MTT Cell Proliferation Assay Kit was used to determine the non-toxic concentration range of test compounds on RAW 264.7 and Hepa-1c1c7 cells following the manufacturer's instructions. Cells were incubated for 24 h in a 96-well microplate at a density of 1 × 10<sup>4</sup> cells/well, followed by the addition of test compounds at a concentration range: of 0.39 to 100 µM. The cell viability was calculated using Equation (1), and the results are presented as the mean ± SD of triplicate.

$$\text{Percent (\%)} \text{ cell viability} = \left( \frac{\text{Optical Density}_{\text{treated}}}{\text{Optical Density}_{\text{untreated}}} \right) \times 100 \quad (1)$$

MTT reagent was added at 10 µL per well under dark conditions, and the cells were incubated for 4 h. Upon incubation, the contents in all wells were aspirated, and DMSO was added at 100 µL per well. The absorbance was measured at 570 nm (630 nm as reference) using a Molecular Devices Spectramax M3 Multi-Mode microplate reader; Sunnyvale, CA, USA. The MTT assay at each concentration was performed in triplicates. The replicates of microplates were carried out to confirm the results.

### Fluorescence polarisation assay

The effect of THBTs in inhibiting Keap1-NRF2 binding was determined using a Keap1-NRF2 inhibitor screening assay kit (BPS Bioscience, USA) following the instructions in the product insert in a 96-well plate. The THBTs were dissolved in molecular biology grade DMSO and diluted with assay buffer provided in the assay kit. Five microlitres of the THBT solutions were incubated at room temperature for 30 min in the peptide mixture containing 0.5 µL NRF2 peptide (1 µM) and 20 µL Keap1 (15 ng/µL). The fluorescence polarisation (FP) was measured using a microplate reader at λ<sub>ex</sub> = 485 nm and λ<sub>em</sub> = 530 nm. The FP values of the blank wells, consisting of only assay buffer, were subtracted from other values. The relative FP intensity of the NRF2 positive control and THBT solutions was measured with reference to the NRF2 negative control. The effect of the THBT compounds in inhibiting Keap1-NRF2 interaction was calculated using Equation (2).

$$\text{Keap1 – Nrf2 inhibitory activity (\%)} = \left( 1 - \frac{\text{Relative FP of THBT}}{\text{Relative FP of positive control}} \right) \times 100 \quad (2)$$

### NRF2 activation activity

#### Effect of THBT on NQO1 activity in Hepa1c1c7 cells

The determination of NQO1 activity was carried out using "Prochaska" Microtiter Plate Bioassay for Inducers of NQO1. This well-established method was reported by Fahey et al.<sup>[28]</sup> using hepatoma cells (Hepa-1c1c7). Hepatoma cells (1 × 10<sup>4</sup> cells/well) were seeded into a 96-well plate and incubated with THBTs at 100–0.78 µM for 48 h. Upon incubation, the medium was discarded, and the cells were washed with PBS. Firstly, the treated cells were lysed with 75 µL digitonin solution. From the cell lysate, 20 µL were used to determine the protein concentration using Bradford's reagent, while 55 µL were used to determine the NQO1 activity. The assay reagent mixture comprised 200 µL 0.5 M Tris-Cl buffer containing 10% w/v bovine serum albumin and 1.5% v/v Tween-20, 7.5 mM FAD, 150 mM glucose-6-phosphate 150 mM, 2 U mL<sup>-1</sup> glucose-6-phosphate dehydrogenase, 50 mM NADP<sup>+</sup>, 25 mM menadione and 0.7 mM MTT. The reaction mixture was mixed with the cell lysate and incubated at 37°C for 5 min to develop purple colour. Next, dicumarol suspension (50 µL; 0.3 mM dicumarol, 5 mM potassium phosphate, 0.5% DMSO) was added to stop the reaction. The optical density of the solution was measured at 610 nm using a Spectramax M3 microplate reader and was normalised to the total protein content.

### Anti-inflammatory activity of test compounds in LPSEc stimulated RAW 264.7 cells

RAW 264.7 cells ( $3 \times 10^5$  cells/well) were seeded in a 96-well microplate with complete media. The cells were allowed to adhere for 24 h. The cells were treated with test compounds 4 h before LPS<sub>Ec</sub> ( $100 \text{ ng mL}^{-1}$ ) stimulation and incubated further for 20 h at  $37^\circ\text{C}$  under a 5% CO<sub>2</sub> incubator. At the end of the experiment, the levels of NO, pro-inflammatory mediators (IL-1 $\beta$ , IL-6, TNF- $\alpha$ , IFN- $\gamma$  and PGE2) were determined from the supernatant solution; while the levels of inflammatory regulators (NF- $\kappa$ B and COX-2) were determined from the cell pellets.

#### Griess assay

Griess assay was prepared by mixing equivalent volumes of 1% (w/v) sulphanilamide in 5% (w/v) phosphoric acid and 0.1% (w/v) of N-(1-naphthyl)ethylenediamine (NED) in water. The standard sodium nitrate (NaNO<sub>2</sub>,  $\geq 97.0\%$ ; Sigma Aldrich, USA) was used as a reference to plot the standard curve. The optical density was measured at 540 nm using a Molecular Devices Spectramax M3 Multi-Mode microplate reader (Sunnyvale, CA, USA). The percentage of NO production concerning (w.r.t.) LPS<sub>Ec</sub> was calculated using Equation (3). The experiment to determine the percentage NO production of test compounds was repeated twice, each performed in triplicate.

$$\text{NO inhibition (\%)} = \left[ 1 - \frac{\left( \text{Optical Density}_{\text{treated}} - \text{Optical Density}_{\text{blank}} \right)}{\left( \text{Optical Density}_{\text{LPS}_{\text{Ec}}} - \text{Optical Density}_{\text{blank}} \right)} \right] \times 100 \quad (3)$$

From the dose-response curve, the concentration of the test compounds to reduce the LPS<sub>Ec</sub> induced NO production by half (IC<sub>50</sub>) was calculated, and the results are presented as mean  $\pm$  SD of two experiments.

#### Effect of test compounds at 50 $\mu\text{M}$ on pro-inflammatory mediators (IL-1 $\beta$ , IL-6, IFN- $\gamma$ , TNF- $\alpha$ , and PGE2) expression in LPSEc-stimulated RAW 264.7 cells

The cell supernatant was collected, and the quantification of pro-inflammatory mediators was measured using Single-Analyte ELISA kits (Qiagen, Germany) containing 96-well plates pre-coated with target-specific capture antibody the manufacturer's instructions using. The OD values and standard reference curve deduce the pro-inflammatory cytokine levels (pg/ml). The fold change in cytokine expression was calculated using Equation (4), and the results are presented as mean  $\pm$  SD from two experiments.

$$\text{Fold change} = \frac{\text{inflammatory mediator level}_{\text{LPS}_{\text{Ec}} \text{ or treated cells}}}{\text{inflammatory mediator level}_{\text{untreated cell}}} \quad (4)$$

#### NF- $\kappa$ B/COX-2 assay

The COX-2 and NF- $\kappa$ B level was measured in the cell lysate of RAW 264.7 following the manufacturer's instructions using 96well plates pre-coated with target-specific immobilised antibody (Abcam, abID# ab210574 and abID# ab176648, respectively). The OD values and standard reference curve determined the pro-inflammatory cytokine levels ( $\text{ng mL}^{-1}$ ). The fold change in cytokine expression was calculated using Equation (5), and the results are presented as mean  $\pm$  SD from two experiments.

$$\text{Fold change} = \frac{\text{NF} - \text{KB or COX} - 2 \text{ level in treatment cells}}{\text{NF} - \text{KB or COX} - 2 \text{ level in LPSEc cells}} \quad (5)$$

#### NRF2 Gene Expression Profiling

The primers for the NQO1, HO-1, and  $\beta$ -actin genes were designed using the Integrated DNA Technologies (IDT) PrimerQuest™ Tool. (<https://sg.idtdna.com/pages/tools/primerquest>) and further confirmed with the reported literature.<sup>[41]</sup> The primer forward and reverse sequences used in this experiment are shown in Table 5.

RNA was isolated from the Hepa-1c1c7 cells using the RNeasy® Mini Kit (Qiagen, Germany; Catalogue number: 74004) according to the manufacturer's protocol. The purity of the isolated RNA was determined using NanoQuant Plate™ (Tecan Trading AG, Switzerland) and Spectramax M3 Multi-Mode microplate reader (Molecular Devices, Sunnyvale, USA). The nucleic acid purity in the isolated RNA was determined by assessing the 260/280 ratio (ideal range:  $\sim 2.0$ ) and 260/230 (ideal range: 2.0–2.2). The purified RNA samples were first converted into cDNA using the ReverTra Ace™ qPCR RT Master Mix with gDNA remover (Toyobo, Japan; catalogue number: FSQ-301). Next, qPCR was performed in a CFX96 thermal cycler (Bio-Rad Laboratories, CA, USA) using THUNDERBIRD Next SYBR® qPCR Mix (Toyobo, Japan; Catalogue number: QPX-201) with the PCR cycling conditions: 1) pre-denaturation step at  $95^\circ\text{C}$  for 60 s, 2) 40 cycles of denaturation at  $95^\circ\text{C}$  for 15 s, followed by annealing at  $60^\circ\text{C}$  for 30 s, and 3) extension at  $72^\circ\text{C}$  for 55 s. The relative changes in gene expression were calculated using the  $2^{-\Delta\Delta\text{CT}}$  method with results normalised to the reference gene,  $\beta$ -actin.

#### Metabolic Stability of THBT compounds

The metabolic stability of THBTs was determined using human, rat, and mouse liver microsomes. Firstly, 5  $\mu\text{L}$  of THBTs ( $0.5 \mu\text{M}$  effective concentration (EC)) was mixed well with 445  $\mu\text{L}$  of liver microsomes ( $0.5 \text{ mg mL}^{-1}$ ). Verapamil ( $0.5 \text{ m EC}$ ) was used as the positive control in this experiment. The mixture was added 50  $\mu\text{L}$  of NADPH (1 mM) in a microcentrifuge tube and was incubated at  $37^\circ\text{C}$  for 0, 3, 6, 15, 30, 45, and 60 min. At each time point, 20  $\mu\text{L}$  of the mixture was sampled and quenched with 180  $\mu\text{L}$  of acetonitrile with internal standard (Donepezil  $50 \text{ ng mL}^{-1}$ ) to terminate the metabolic reaction. Ultrapure water (80  $\mu\text{L}$ ) was added, and contents in the microcentrifuge tubes were centrifuged at 3800 rpm at  $4^\circ\text{C}$  for 10 min. After centrifugation, the concentration of THBTs found in the supernatant layer was quantified using Agilent 1290 coupled with Q-TOF. Each set of experiments was repeated three times in human, rat, and mouse liver microsomes. The THBTs concentration versus time was plotted to determine the elimination rate constant ( $K_{\text{el}}$ ). The intrinsic clearance ( $Cl_{\text{int}}$ ) and half-life ( $t_{1/2}$ ) were calculated using Equation (6) and Equation (7), respectively. The intrinsic clearance was calculated with scaling factors of microsomal protein ( $52.5 \text{ mg microsomal protein/g liver}$ ).<sup>[42]</sup>

**Table 5.** Primer pair sequences for NQO1, HO-1, and  $\beta$ -Actin genes.

Gene	Gene Sequence	
NQO1	Forward	GAGAAGAGCCCTGATTGTACTG
	Reverse	ACCTCCCATCCTCTCTTCTT
HO-1	Forward	GATGATGGAGCGTCCACAGC
	Reverse	TTGGTGGCCTCCTCAAGG
$\beta$ -Actin	Forward	CGGTTCCGATGCCCTGAGGCTCTT
	Reverse	CGTCACACTTCATGATGGAATTGA

$$Cl_{int} = \frac{K_{el}}{0.5} \times 52.5 \quad (6)$$

$$t_{1/2} = \frac{0.693}{K_{el}} \quad (7)$$

### Statistical analysis

The results were represented as mean  $\pm$  SD ( $n=3$ ). The statistical analyses were carried out using GraphPad Prism 9.0.0. The significance was calculated using ordinary ANOVA, followed by the Dunnett test. The four levels of significance were determined.  $p < 0.05$  is denoted as \*,  $p < 0.01$  is denoted as \*\*,  $p < 0.001$  is denoted as \*\*\*, and  $p < 0.0001$  is denoted as \*\*\*\*.

### Molecular docking studies

The in silico molecular docking studies were carried out using Schrödinger Drug Discovery Suite (2021-4) according to the instructions described in the user manual. The structures of the compounds were drawn using a 2D sketcher and imported into Maestro as 3D structures. The structures were minimised using the 'LigPrep' wizard at pH  $7.2 \pm 0.2$ . The protein crystal structure (PDB ID: 4IQK) was downloaded from the RCSB PDB website (<https://www.rcsb.org/>). The protein was prepared using the 'protein preparation' wizard at pH  $7.2 \pm 0.2$  with default settings. The grid was generated around the inbound ligand using the 'receptor grid generation' tool with default settings. Following the extra precision (XP) protocol, the compounds were docked into the receptor grid using the 'GLIDE' wizard. The docking protocol was validated by determining the RMSD between the poses of the co-crystallised ligand and the docked ligand. The interactions between the compounds and the amino acid residues in the receptor were generated using a 2D interaction diagram tool. The 2D and 3D interactions were captured as images.

### Prediction of binding free energies

Prime MM-GBSA was used to predict the free energy of binding between the receptor and the compounds.<sup>[43]</sup> The binding free energy ( $DG_{bind}$ ) was calculated using the default parameters. The docked complexes were used as input files with implicit VSGB solvation model, OPLS3 force field, and all other settings as default in Prime MM-GBSA. The binding free energy of the compounds is calculated using Equation (8):<sup>[44]</sup>

$$\Delta G_{bind} = E_{complex}(\text{minimised}) - (E_{ligand}(\text{minimised}) + E_{receptor}(\text{minimised})) \quad (8)$$

### Molecular dynamics (MD) simulation

MD simulations were performed with the Desmond package in Schrödinger Drug Discovery Suite. The selected compound-receptor complexes were first immersed in SPC (simple point charge) water box, extending 10 Å beyond any of the complex's atoms. Counter ions (33 Na<sup>+</sup>, and 29 Cl<sup>-</sup> ions) were added to neutralize charges. The MD was performed in the NPT ensemble at a temperature of 300 K and 1.63 bar pressure over 20 ns with recording intervals of 1.2 ps for energy and 100 ns for trajectory. Simulations were run with the OPLS-3e force field. The root means square deviation (RMSD), root means square fluctuations (RMSF), and ligand contacts

were obtained to monitor the stability of the compounds in their dynamic form along with simulated trajectory.

### Prediction of physicochemical and drug-likeness properties

The ADMET and drug-likeness properties of the compounds were predicted using the QikProp module with default settings.

### Acknowledgements

The authors wish to thank the International Medical University, Kuala Lumpur, Malaysia, for financial support [Project ID: PMHS I-2018 (02); IMUR422/2018].

### Conflict of Interest

The authors declare no conflict of interest.

### Data Availability Statement

The data that support the findings of this study are available in the supplementary material of this article.

**Keywords:** anti-inflammatory · NRF2 activators · tetrahydrobenzothiophene · thiophenes

- [1] L. Chen, H. Deng, H. Cui, J. Fang, Z. Zuo, J. Deng, Y. Li, X. Wang, L. Zhao, *Oncotarget* **2018**, *9*, 7204–7218.
- [2] A. Ortega-Gómez, M. Perretti, O. Soehnlein, *EMBO Mol. Med.* **2013**, *5*, 661–74.
- [3] A. Cuadrado, A. I. Rojo, G. Wells, J. D. Hayes, S. P. Cousin, W. L. Rumsey, O. C. Attucks, S. Franklin, A.-L. Levenon, T. W. Kensler, A. T. Dinkova-Kostova, *Nat. Rev. Drug Discovery* **2019**, *18*, 295–317.
- [4] A. T. Dinkova-Kostova, A. Y. Abramov, *Free Radical Biol. Med.* **2015**, *88*, 179–188.
- [5] E. Kansanen, S. M. Kuosmanen, H. Leinonen, A.-L. Levenon, *Redox Biol.* **2013**, *1*, 45–9.
- [6] A. J. Wilson, J. K. Kerns, J. F. Callahan, C. J. Moody, *J. Med. Chem.* **2013**, *56*, 7463–7476.
- [7] S. M. U. Ahmed, L. Luo, A. Namani, X. J. Wang, X. Tang, *Biochim. Biophys. Acta Mol. Basis Dis.* **2017**, *1863*, 585–597.
- [8] S. Saha, B. Buttari, E. Panieri, E. Profumo, L. Saso, *Molecules* **2020**, *25*, 5474.
- [9] X. Sun, Y. Yang, J. Shi, C. Wang, Z. Yu, H. Zhang, *J. Appl. Toxicol.* **2017**, *37*, 1428–1437.
- [10] N. D. Georgakopoulos, S. K. Talapatra, J. Gatliff, F. Kozielski, G. Wells, *ChemBioChem* **2018**, *19*, 1810.
- [11] A. Kobayashi, M.-I. Kang, Y. Watai, K. I. Tong, T. Shibata, K. Uchida, M. Yamamoto, *Mol. Cell. Biol.* **2006**, *26*, 221–9.
- [12] N. F. Villeneuve, A. Lau, D. D. Zhang, *Antioxid. Redox Signaling* **2010**, *13*, 1699–712.
- [13] V. Krajka-Kuźniak, J. Paluszczak, W. Baer-Dubowska, *Pharmacol. Rep.* **2017**, *69*, 393–402.
- [14] E. H. Kobayashi, T. Suzuki, R. Funayama, T. Nagashima, M. Hayashi, H. Sekine, N. Tanaka, T. Moriguchi, H. Motohashi, K. Nakayama, M. Yamamoto, *Nat. Commun.* **2016**, *7*, 11624.
- [15] X. Wang, M. Li, Y. Cao, J. Wang, H. Zhang, X. Zhou, Q. Li, L. Wang, *Eur. J. Pharmacol.* **2017**, *809*, 196–202.
- [16] Q. Lin, X. Qin, M. Shi, Z. Qin, Y. Meng, Z. Qin, S. Guo, *Int. Immunopharmacol.* **2017**, *49*, 142–147.
- [17] D. D. Zhang, M. Hannink, *Mol. Cell. Biol.* **2003**, *23*, 8137–8151.

- [18] V. Nagaveni, S. Prabhakar, *Rapid Commun. Mass Spectrom.* **2015**, *29*, 1155–1164.
- [19] Y. Zhang, A. Gilmour, Y.-H. Ahn, L. de la Vega, A. T. Dinkova-Kostova, *Phytomedicine* **2019**, DOI 10.1016/j.phymed.2019.153062.
- [20] S. R. Baier, R. Zbasnik, V. Schlegel, J. Zempleni, *J. Nutr. Biochem.* **2014**, *25*, 665–668.
- [21] X. G. Huang, J. Liu, J. Ren, T. Wang, W. Chen, B. B. Zeng, *Tetrahedron* **2011**, *67*, 6202–6205.
- [22] R. W. Sabnis, D. W. Rangnekar, N. D. Sonawane, *J. Heterocycl. Chem.* **1999**, *36*, 333–345.
- [23] K. Gewald, *Chem. Heterocycl. Compd.* **1976**, *12*, 1077–1090.
- [24] T. Miyazawa, M. Yamamoto, Y. Maeda, *Synthetic Communications* **2009**, *39*, 1092–1099.
- [25] S. Thanna, S. E. Knudson, A. Grzegorzewicz, S. Kapil, C. M. Goins, D. R. Ronning, M. Jackson, R. A. Slayden, S. J. Sucheck, *Org. Biomol. Chem.* **2016**, *14*, 6119–6133.
- [26] E. M. Gad, M. S. Nafie, E. H. Eltamany, M. S. A. G. Hammad, A. Barakat, A. T. A. Boraie, *Molecules* **2020**, *25*, 2523.
- [27] G. Guedes de La Cruz, B. Svobodova, M. Lichtenegger, O. Tiapko, K. Groschner, T. Glasnov, *Synlett* **2017**, *28*, 695–700.
- [28] J. W. Fahey, A. T. Dinkova-Kostova, K. K. Stephenson, P. Talalay, *Methods Enzymol.* **2004**, *382*, 243–258.
- [29] A. T. Dinkova-Kostova, J. W. Fahey, R. V. Kostov, T. W. Kensler, *Trends Food Sci. Technol.* **2017**, *69*, 257–269.
- [30] K.-K. Mak, Z. Shiming, M. K. Balijepalli, A. T. Dinkova-Kostova, O. Epemolu, Z. Mohd, M. R. Pichika, *Phytomedicine Plus* **2021**, *1*, 100018.
- [31] J. S. Yuan, A. Reed, F. Chen, C. N. Stewart, *BMC Bioinf.* **2006**, *7*, 1–12.
- [32] M. Kandasamy, K.-K. Mak, T. Devadoss, P. V. Thanikachalam, R. Sakirolla, H. Choudhury, M. R. Pichika, *BMC Chemistry*. **2019**, *13*, 117.
- [33] J. M. Zhang, J. An, *Int. Anesthesiol. Clin.* **2007**, *45*, 27–37.
- [34] D. M. Brown, K. Donaldson, V. Stone, *J. Biomed. Nanotechnol.* **2010**, *6*, 224–33.
- [35] W. Langhans, in *Cachexia Wasting A Mod. Approach*, Springer Milan, **2007**, pp. 209–217.
- [36] E. Ricciotti, G. A. Fitz Gerald, *Arterioscler. Thromb. Vasc. Biol.* **2011**, *31*, 986–1000.
- [37] M. Davies, R. D. O. Jones, K. Grime, R. Jansson-Löfmark, A. J. Fretland, S. Winiwarter, P. Morgan, D. F. McGinnity, *Trends Pharmacol. Sci.* **2020**, *41*, 390–408.
- [38] D. C. Ackley, K. T. Rockich, T. R. Baker, in *Optim. Drug Discov.*, Humana Press, Totowa, NJ, **2004**, pp. 151–162.
- [39] R. A. Friesner, R. B. Murphy, M. P. Repasky, L. L. Frye, J. R. Greenwood, T. A. Halgren, P. C. Sanschagrin, D. T. Mainz, *J. Med. Chem.* **2006**, *49*, 6177–6196.
- [40] N. Patel, O. Hatley, A. Berg, K. Romero, B. Wisniowska, D. Hanna, D. Hermann, S. Polak, *AAPS J.* **2018**, *20*, 1–13.
- [41] A. P. Zarecki, J. L. Kolanowski, W. T. Markiewicz, *Molecules* **2020**, *25*, 1761.
- [42] T. Iwatsubo, N. Hirota, T. Ooie, H. Suzuki, N. Shimada, K. Chiba, T. Ishizaki, C. E. Green, C. A. Tyson, Y. Sugiyama, *Pharmacol. Ther.* **1997**, *73*, 147–171.
- [43] S. Genheden, U. Ryde, *Expert Opin. Drug Discovery* **2015**, *10*, 449–61.
- [44] T. Hou, J. Wang, Y. Li, W. Wang, *J. Chem. Inf. Model.* **2011**, *51*, 69–82.

---

Manuscript received: August 12, 2022

Revised manuscript received: September 11, 2022